Photonic-assisted Broadband RF Receivers with Low IF Frequencies Based on Kramers-Kronig Processing

Lu, Bing; Bai, Yifan; Zhang, Jiaxin; Tang, Jianming; Guo, Pengxing; Hou, Weigang; Guo, Lei

Optics Express

DOI:
10.1364/OE.545893

Published: 24/02/2025

Publisher's PDF, also known as Version of record

Research Article Vol. 33, No. 5 / 10 Mar 2025 / Optics Express 9176
Optics EXPRESS

Photonic-assisted broadband RF receivers with low IF frequencies based on Kramers-Kronig processing

BING LU,[1,2,3,*] YIFAN BAI,[1,2] JIAXIN ZHANG,[1,2] JIANMING TANG,[3] PENGXING GUO,[1,2] WEIGANG HOU,[1,2] AND LEI GUO[1,2]

[1]School of Communications and Information Engineering, Chongqing University of Posts and Telecommunications, Chongqing 400065, China
[2]Institute of Intelligent Communications and Network Security, Chongqing University of Posts and Telecommunications, Chongqing 400065, China
[3]Digital Signal Processing Centre of Excellence, School of Computer Science and Engineering, Bangor University, Bangor LL57 1UT, United Kingdom
*lubing@cqupt.edu.cn

Abstract: A simplified photonic-based radio frequency (RF) receiver with a low intermediate frequency (IF) is proposed and experimentally demonstrated by utilizing direct detection and Kramers-Kronig (KK) processing. In the proposed approach, the RF and local oscillator (LO) signals are modulated onto an optical carrier using a dual-drive Mach-Zehnder modulator (DDMZM) biased at a minimum transmission point. The modulated optical signal is then directed to a single photodetector (PD) to produce the IF signal, which is designed to fall within 1.5 times the bandwidth of the RF signal. KK processing effectively mitigates the signal-signal beat interference (SSBI) when the frequency gap between the RF signal and the LO signal is 1.5 times less than the bandwidth of the RF signal, thus enabling the generation of a low IF signal. This allows for subsequent processing with a low-speed PD and an analog-to-digital converter operating at a lower sampling rate. Experimental validation using a 16-QAM RF vector signal shows that KK processing reduces the error vector magnitude (EVM) of the down-converted 16-QAM signal to 4.61%, compared to 18.57% without it when no frequency gap exists. This approach provides a streamlined design and straightforward implementation for photonic RF down-conversion.

1. Introduction

Radio frequency (RF) receivers play a pivotal role in modern communications, radar and satellite communications, enabling the reception and processing of signals transmitted over various frequencies [1–3]. With the advancement of communication and radar technologies, the frequencies of radio signals are moving towards higher carriers to gain a large bandwidth [4–9]. For instance, modern applications such as 5 G and future 6 G networks require wide bandwidths to support ultrafast data transmissions, great connection densities, and improved spectral efficiencies, while in radar systems, high-resolution imaging technologies also rely on increased bandwidths to achieve improved resolutions, high sensitivities, and more robust signal processing capabilities. Therefore, there is a pressing need for RF receivers to operate across diverse frequency bands within a wideband frequency coverage. However, limited by electronic bottlenecks, traditional electronic RF receivers face significant challenges in terms of limited bandwidth, fragility to electromagnetic interference (EMI), and high-power consumption at high frequencies.

Microwave photonic RF receivers offer a compelling solution by leveraging the advantages of photonic technologies including ultra-wide bandwidth, low loss, and immunity to electromagnetic

#545893 https://doi.org/10.1364/OE.545893
Journal © 2025 Received 24 Oct 2024; revised 3 Feb 2025; accepted 6 Feb 2025; published 24 Feb 2025

Optics EXPRESS

interference [1,2,7,9,10]. Among these advantages, broadband RF down-conversion is essential to the RF receivers, which translates RF signal to an intermediate frequency (IF) or baseband signal by mixing it with a local oscillator (LO) signal. It bridges the gap between high-frequency signal acquisition and low-frequency processing, thus enabling low-speed analog and digital circuits to operate efficiently and accurately. Over the past few years, various photonic-assisted RF down-conversion approaches have been proposed and demonstrated, of which the most widely used methods are to modulate the RF and LO signals into an optical carrier by utilizing an electro-optic modulator (EOM) [11,12], cascaded [13–15] or parallel [16–23] structures. After square-law detection by a single photodetector (PD), the desired IF signal is obtained. However, in these schemes, the frequency gap between the RF signal and the LO signal needs to be >1.5 times larger than the bandwidth of the RF signal, in order to avoid signal-signal beating interference (SSBI) within the signal spectral region [24,25]. SSBI arises in direct detection systems due to the square-law nature of PD, where signal-signal beating produces unwanted mixing products that interfere with the desired signal-carrier beat terms. If this frequency gap is insufficient, these mixing products will overlap with the down-converted IF signal, causing distortion and significantly reducing receiver sensitivity [26]. Additionally, the rapid growth in RF bandwidth, driven primarily by modern communications and radar systems, further increases the required frequency gap. This will result in increased bandwidth requirements for processing the IF signal, thus giving rise to enhanced hardware complexity and cost. Photonic down-conversion based on balanced detection is an effective technique for mitigating SSBI [27–33]. Typically, the RF-encoded optical signal and the optical LO tone are separately routed to an optical coherent receiver, which consists of a 90-degree optical hybrid coupler and balanced PDs [27–31]. However, the optical coherent receivers are costly, power-hungry, and sensitive to noise and laser linewidth. Other configurations, such as utilizing a dual polarization division multiplexing Mach-Zehnder modulator (MZM) combined with balanced detection, can achieve RF downcoversion with SSBI suppression [32–34]. However, they encounter stability issues, as the polarization states are sensitive to environmental vibrations, and solving these issues often requires sophisticated polarization control and compensation techniques, which introduces extra complexity to the system [35].

The Kramers-Kronig (KK) algorithm has recently gained significant attention because of its effectiveness in mitigating SSBI, enabling the recovery of signal phase from intensity-only information in direct detection systems [26,36–38]. A photonic low IF RF receiver utilizing two dual-parallel dual-drive MZM (DP-DDMZM) has been reported, where RF and LO signals are loaded onto an optical carrier via carrier-suppression single sideband (CS-SSB) modulation, and the low IF signal is recorrected using KK detection [39]. However, this scheme relies on two wideband RF quadrature hybrids, which suffer from frequency-dependent responses, thereby limiting the system's operating frequency and bandwidth. Furthermore, both accurate path length matching and a narrow laser linewidth are also essential. An alternative approach involves a DP-DDMZM with a CS-DSB modulation and KK processing to create a photonic RF low IF receiver [40]. This design reduces the system complexity by eliminating the need for RF hybrids and using only a single modulator. However, the DP-DDMZM consists of two nested MZMs and a parent MZM, requiring at least two bias controllers to stabilize the bias points, which adds additional complexity to implementing CS-DSB modulation for both paths. Additionally, it also suffers from a large insertion loss and footprint.

In this paper, we propose a simplified low-IF RF receiver based on a DDMZM biased at the minimum transmission point (MITP) and KK processing. Compared to previous works [39] and [40], our approach further reduces system complexity by eliminating the need for additional optical components while maintaining effective signal recovery. Additionally, our work demonstrates the feasibility of low-IF reception with KK detection in a more compact and practical configuration. RF and LO signals are fed into the two RF ports of the DDMZM. By

Optics EXPRESS

precisely adjusting the DDMZM's bias voltage at the MITP, the desired IF signal is generated. KK detection effectively mitigates SSBI, enhancing the reception of low IF signals. Experimental results validate the receiver's performance for low IF signals by comparing the error vector magnitude (EVM) of down-converted IF signals with and without KK detection. The results show significant EVM improvements when KK detection is used, particularly when the IF signal frequency is less than 1.5 times of the bandwidth of the RF signal.

2. Principle

Figure 1 presents a schematic diagram of the proposed RF receiver with a low IF. Firstly, the RF and LO signals are fed into a DDMZM for up-conversion, which have been demonstrated superior performances in [16,41]. After passing through an erbium-doped fiber amplifier (EDFA) and a tunable optical filter (TOF), the PD-detected real-valued electrical signal consists of both the desired down-converted signal and SSBI. Next, the reconstruction of a corresponding complex signal is performed on a digital signal processor (DSP) using KK processing to eliminate SSBI. This enables the effective reception at a low IF. The detailed theoretical analysis of the above-described process is given below.

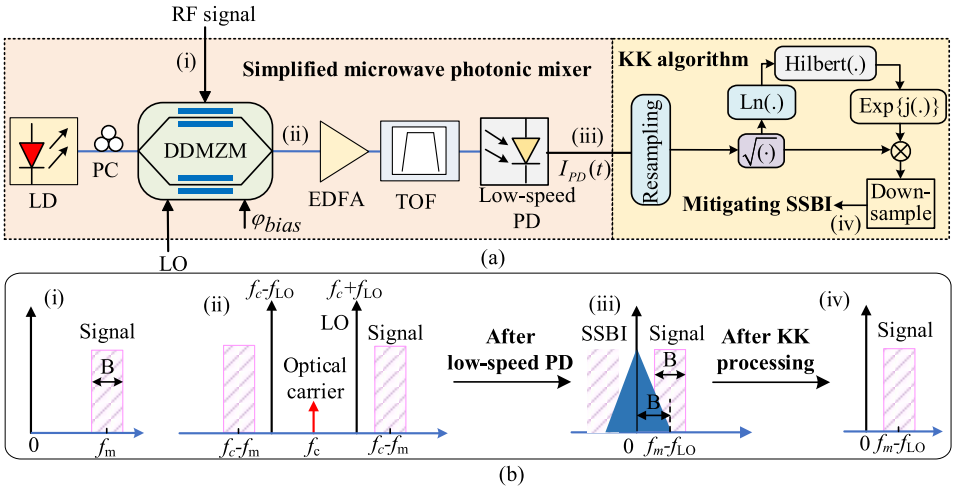

Fig. 1. Schematic diagram of the proposed system. LD: laser diode; DDMZM: dual-driven Mach-Zehnder modulator; EDFA: erbium-doped fiber amplifier; TOF: tunable optical filter; PD: photodiode; KK: Kramers-Kronig; SSBI: signal-signal beating interference.

According to Fig. 1, an optical continuous wave with a frequency ω_0 is generated by a laser diode (LD), denoted as $E_{in}(t) = E_{in}\exp(j\omega_0 t)$, which is sent to the DDMZM via passing through a polarization controller (PC) with a half-wave voltage of V_π. As the RF and LO signals are loaded on the RF ports of the DDMZM, the output light field can be expressed by

$$E_{out}(t) = E_{in}(t)\left\{\exp\left[\frac{j\pi[V_{DC1} + V_{RF}(t)\cos(\omega_{RF}t)]}{V_\pi}\right] + \exp\left[\frac{j\pi[V_{DC2} + V_{LO}\cos(\omega_{LO}t)]}{V_\pi}\right]\right\} \quad (1)$$

where V_{DC1}, V_{DC2} are bias voltages of the upper and the lower arms, $V_{RF}(t)$ and V_{LO} are the amplitudes of the RF and LO signals, ω_{RF} and ω_{LO} are the angle frequencies of the RF and LO signals. Under the small-signal modulation, Eq. (1) can be expanded using a Taylor series as

$$E_{out}(t) = E_{in}(t)\cdot\exp\left(j\frac{\pi V_{DC2}}{V_\pi}\right)\cdot\left\{\begin{array}{l}\exp(j\Delta\varphi)[1 + j\frac{\pi V_{RF}(t)\cos(\omega_{RF}t)}{V_\pi} + O(X^2)] \\ +[1 + j\frac{\pi V_{LO}\cos(\omega_{LO}t)}{V_\pi} + O(X^2)]\end{array}\right\} \quad (2)$$

Optics EXPRESS

where $\Delta\varphi = \pi(V_{DC1} - V_{DC2})/V_\pi$ is the phase shift deviation introduced by the bias voltage of the two arms, $\beta_1 = \pi V_{LO}/V_\pi$ is the modulation index of the lower arm, $O(X^2)$ represents the second-order nonlinear distortion (NLD) obtained through Taylor expansion, with the third-order and higher NLD terms omitted. When the optical signal in Eq. (2) is sent to a PD, the resulting electrical signal can be expressed as

$$\begin{aligned} I_{DSB}(t) \propto P_{in}[2 + 2\cos\Delta\varphi + \frac{\beta_1^2}{2} + \frac{\pi^2}{2V_\pi^2}V_{RF}^2(t) + \frac{\pi}{V_\pi}\beta_1 V_{RF}(t)\cos\Delta\varphi\cos(\omega_{RF} - \omega_{LO})t \\ + \frac{\pi}{V_\pi}\beta_1 V_{RF}(t)\cos\Delta\varphi\cos(\omega_{LO} + \omega_{RF})t + 2\sin\Delta\varphi\cos(\omega_{LO}t) - 2\sin\Delta\varphi\cos(\omega_{RF}t) \\ + \frac{\pi^2}{2V_\pi^2}V_{RF}^2(t)\cos(2\omega_{RF}t) + \frac{\beta_1^2}{2}\cos(2\omega_{LO}t) + O(X^2)(2 + 2\cos\Delta\varphi) + \ldots.] \end{aligned} \quad (3)$$

where $P_{in} = |E_{in}(t)|^2$ is the power of the optical carrier, $P_{in}[2 + 2\cos\Delta\varphi + \beta_1^2/2]$ is the direct currency (DC) term generated by self-beating of the optical LO signals and the optical carrier, $P_{in}\pi^2 V_{RF}^2(t)/2V_\pi^2$ is the SSBI, $\pi/V_\pi[P_{in}\beta_1 V_{RF}(t)\cos\Delta\varphi\cos(\omega_{RF} - \omega_{LO})t]$ is the desired down-converted IF signal, and remaining terms are the high-frequency terms generated from the cross-beating between the upper and lower sidebands. It is noteworthy that the down-converted IF component at the frequency of $\omega_{LO} - \omega_{RF}$ depends on the phase $\Delta\varphi$. When $\Delta\varphi = \pi/2$, the amplitude of the IF signal is zero, indicating unsuccessful down-conversion. Conversely, when $\Delta\varphi = 0$ or $\Delta\varphi = \pi$, the IF signal reaches its maximum amplitude, and the unwanted frequency components at ω_{RF} and ω_{LO} are completely eliminated [16]. Additionally, when a low-speed PD is used, the high-frequency components can be filtered out. Under these conditions, and assuming second-order and higher-order NLDs are negligible, Eq. (3) can be rewritten as

$$I_{DSB}(t) \propto P_{in}[2 + 2\cos\Delta\varphi + \beta_1^2/2 + \frac{\pi^2}{2V_\pi^2}V_{RF}^2(t) + \frac{\pi}{V_\pi}\beta_1 V_{RF}(t)\cos(\Delta\varphi)\cos(\omega_{RF} - \omega_{LO})t] \quad (4)$$

To eliminate the DC generated by self-beating of the optical carrier and maintain a high conversion gain, the DC bias is adjusted precisely to satisfy the condition of $\Delta\varphi = \pi$, ensuring the suppression of the optical carrier. Consequently, Eq. (4) can be rewritten as

$$I_{DSB}(t) \propto P_{in}[\frac{\beta_1^2}{2} + \frac{\pi^2}{2V_\pi^2}V_{RF}^2(t) + \frac{\pi}{V_\pi}\beta_1 V_{RF}(t)\cos(\omega_{RF} - \omega_{LO})t] \quad (5)$$

According to Eq. (5), the KK algorithm is employed to mitigate SSBI and also to reconstruct the full complex optical field. The KK algorithm requires the signal to be a minimum-phase signal for accurate recovery, which necessitates a high carrier-to-signal power ratio (CSPR), as indicated in [42].

$$CSPR = 10\log\left(\frac{P_{LO}}{P_S}\right) = 10\log\left(\frac{|E_{LO}|^2}{|E_{s(t)}|^2}\right) \quad (6)$$

where $P_{LO} = |E_{\mathrm{LO}}|^2 = P_{in}\beta_1^2/2$, $P_S = |E_{s(t)}|^2 = P_{in}\pi^2 V_{RF}^2(t)/2V_\pi^2$. To better understand how the KK algorithm mitigates SSBI, we delve further into its theoretical foundation based on the minimum-phase signal assumption. The minimum-phase condition ensures that the amplitude and phase of the signal are inherently linked through a causal relationship, which allows the full reconstruction of the optical field using only intensity information [36,37].

The first step in the KK algorithm is to calculate the logarithm of the detected photocurrent $I_{DSB}(t)$, as shown in Eq. (5). Assuming the signal satisfies the minimum-phase condition, the KK relation ensures that the phase of the optical field $\phi_s(t)$, can be accurately reconstructed using the

Optics EXPRESS

Hilbert transform of $\ln[I_{DSB}(t)]$. Mathematically, this is expressed as

$$\phi_s(t) = \frac{1}{2\pi} p.v. \int_{-\infty}^{\infty} \frac{\ln[I_{DSB}(t')]}{t - t'} dt' \tag{7}$$

where p. v. denotes the Cauchy principal value of the integral. This operation eliminates the need for complex phase measurement, by relying solely on amplitude to recover the phase. According to Eq. (7), its expression in the frequency domain can be written as

$$\widetilde{\phi_s}(\omega) = i * sign(\omega) F\{\ln[|I_{DSB}(t)|]\} \tag{8}$$

where $sign(\omega)$ represents the sign function and $F\{\cdot\}$ denotes the Fourier transform operation. The phase signal $\phi_s(t)$, derived from the inverse Fourier transform operation in the frequency domain, is subsequently transformed back into the time domain, allowing for the reconstruction of the original signal field. The reconstructed optical field can be expressed as

$$\mathrm{I}_s(t) = \left\{ \sqrt{I_{DSB}(t)} \exp[j\phi_s(t)] - E_{LO} \right\} \exp[j(\omega_{RF} - \omega_{LO})t] \tag{9}$$

It is noted that during the reconstruction process, only signals satisfying the minimum-phase condition can be accurately recovered. Since SSBI typically does not meet this condition, it is treated as noise and naturally suppressed. Additionally, the spectral broadening resulting from the logarithmic operations must be addressed by digital up-sampling, which may pose strict demands on the involved digital signal processor and increases the system complexity. Such restrictions can be relaxed using a new DSP algorithm for the KK receiver described in the literature [43].

3. Experimental results

For proof-of-concept experimental demonstrations, the considered experimental setup is illustrated in Fig. 2. A tunable laser source (TLS, EXF T100S-HP) emits an optical wave with a wavelength of 1550.646 nm, a linewidth of 400 kHz, and an optical power of 10 dBm. A PC is placed before the modulator to minimize polarization-related losses. The signal is then fed into a DDMZM (Fujitsu FTM 7937) with a half-wave voltage of 3.5 V and an insertion loss of 5 dB. The RF and LO signals are generated by an arbitrary waveform generator (AWG, Keysight M8196A) and a microwave signal generator (MSG, Prosund SP240), respectively. After electro-optic modulation, the signal is amplified by an EDFA with a constant output power of 12 dBm to compensate for the optical losses. The amplified signal then passes through a TOF (EXFO XTM-50) to filter out-of-band ASE noise. Finally, the optical signal is injected into a PD with a responsivity of approximately 0.8 A/W. An optical spectrum analyzer (OSA, Yokogawa AQ6370D) with a resolution of 0.02 nm is used to monitor and analyze the spectrum of the optical signal, while an oscilloscope (OSC, Tektronix DPO73304SX) recorded and digitized the electrical IF signals generated by photonic down-conversion. The off-line DSP is performed for the full complex signal retrieval and digital demodulation via MATLAB. Before the offline DSP processing, a brick-wall low-pass filter provided by the OCS is applied to eliminate unwanted interferences outside the signal bandwidth. The DSP flow is displayed in the second half of Fig. 2. The digitalized IF signal is firstly resampled, and the complex signal reconstruction is carried out using the KK algorithm to mitigate the SSBI. Next, mean cancellation is applied to the recovered signal to remove the direct current (DC) offset, followed by digital IQ down-conversion and matched filtering to enhance the signal quality. After time synchronization, down-sampling and phase correction are applied to the baseband signal to ensure accuracy and stability. Finally, symbol judgment is performed, and EVMs are calculated to assess the system performance. For comparison, an alternative DSP without the KK algorithm and other processes are unchanged.

A 16-QAM microwave vector signal, centered at 15 GHz, is chosen as the RF signal. The symbol rate is set to be 400 MBaud, and pulse shaping is applied by using a root-raised cosine

Optics EXPRESS

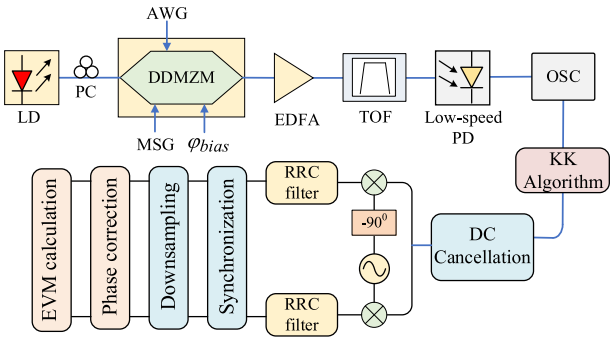

Fig. 2. Experimental setup. AWG: arbitrary waveform generator; ASG: analogue signal generator; OSC: oscilloscope; DC: direct current; RRC: root raised cosine; EVM: error vector magnitude.

(RRC) filter with a roll-off factor of 0.25, yielding a signal bandwidth of 500 MHz. Due to the limitations of the AWG, the RF signal power is controlled by adjusting its peak-to-peak voltage from 500 mV. The LO frequency is set to be 14.5 GHz with a power of 6 dBm. Figure 3(a) illustrates the optical spectrum when only the 16QAM RF signal is applied, with the DDMZM biased at its MITP. Upon introducing the LO signal to the DDMZM, the resulting optical spectrum is shown in Fig. 3(b), where the optical carrier is approximately 10 dB lower than the first sidebands. The performance of the proposed RF receiver for handling lower IF reception using KK detection is subsequently evaluated. The LO frequency is adjusted to 14.25 GHz to ensure the proper separation between the down-converted signal and SSBI. Figure 4(a) and (b) present the normalized power spectrum of the sampled signals obtained by Fast Fourier Transform (FFT). Based on the analysis of data collected from the OSC and calculated using Eq. (6), the CSPR is determined to be 10.93 dB, which satisfies the minimum phase condition. It is evident that the center frequencies of the SSBI and the down-converted signal are 250 MHz and 750 MHz, respectively, both with bandwidths of 500 MHz. Since the SSBI and the desired signal are well-separated in frequency, the desired signal can be demodulated efficiently, resulting in nearly identical EVMs of 4.41% and 4.37% with and without KK processing. The results with and without applying the KK detection are shown in Figs. 4(c) and (d), where the SSBI interference completely overlaps with the IF signal. As shown in Fig. 4(c), due to the spectral overlap between the SSBI and the IF signal, the constellation points of the demodulated IF signal are dispersed around the center, resulting in an EVM of 18.16%. After applying the KK processing, SSBI is mitigated, and the constellation points become more concentrated, with the EVM being improved to 4.87%, which is almost identical to the cases shown in Figs. 4(a) and (b). This clearly demonstrates the effectiveness of the KK algorithm in mitigating SSBI. It is also important to note that the power of the down-converted IF signal is related to the bias stability of the DDMZM, as shown in Eq. (5). Therefore, commercial bias controllers can be used to stabilize the modulator bias in order to further improve the system performance.

The quality of the down-converted signals at different IF frequencies is analyzed utilizing their EVMs. The carrier frequency of the RF signal is kept constant, while varying the LO frequency resulted in different IF center frequencies. Corresponding EVMs are assessed with and without KK detection, and the results are presented in Fig. 5(a). To generalize the experimentally measured developing trends for typical signals, we define the normalized IF as the IF frequency divided by half of the signal bandwidth (i.e., 250 MHz). The results indicate that the EVM decreases as the IF frequency increases, due to reduced spectral overlaps between the signal and the SSBI. However, when the normalized IF center frequency approaches 3 (corresponding to an LO of 14.25 GHz), the EVM remains almost unchanged. With KK detection, the EVM remains

Optics EXPRESS

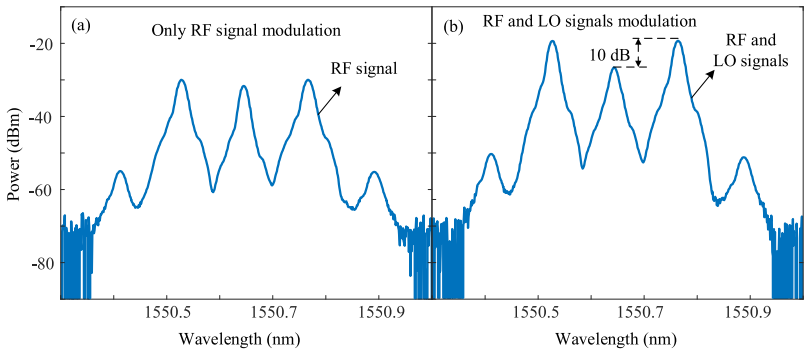

Fig. 3. Optical spectra of CS-DSB signal: (a) only with 16QAM RF modulation, (b) with 16 QAM RF and LO modulation.

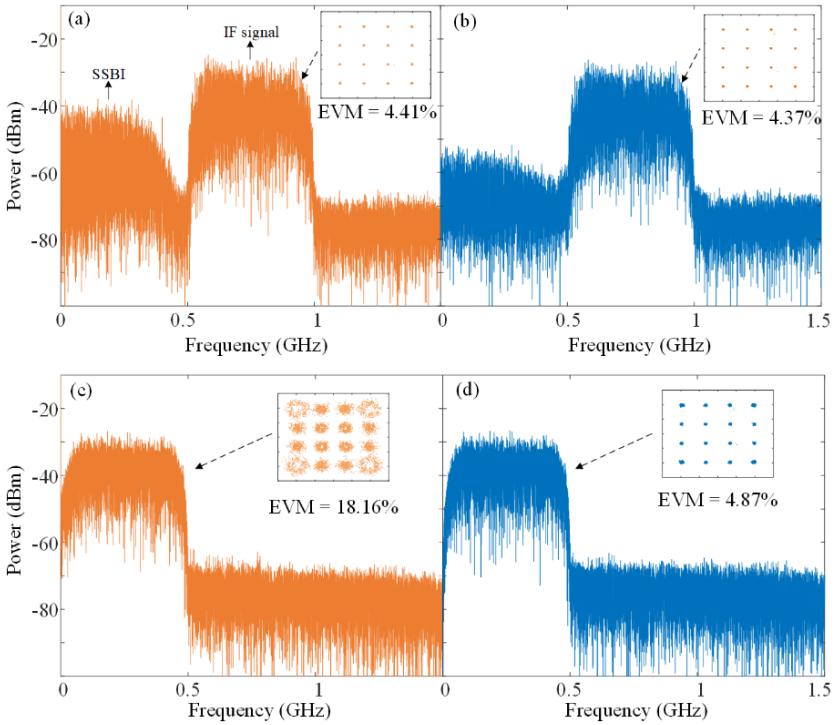

Fig. 4. Power spectrum of the IF signal: Signals separated from SSBI: (a) without KK processing, (b) with KK processing; Signals overlapping with SSBI: (c) without KK processing, (d) with KK processing.

consistently low across different IF frequencies, demonstrating its effectiveness in suppressing the SSBI, even in the presence of spectral overlaps. Notably, the EVM decreases from 18.57% to 4.61% at a normalized IF frequency of 1, highlighting the strong reception performances at lower IF frequencies. The variation of EVM with LO signal power is demonstrated in Fig. 5(b), where the peak-to-peak voltage of the 16QAM signal is fixed at 500 mV. The CSPRs are derived from Eq. (6) and calculated to be 10.93 dB, 11.21 dB, 11.43 dB, 11.63 dB, 11.95 dB, 12.22 dB, 12.85 dB and 13.05 dB, respectively. It is important to note that each of these CSPRs satisfies its corresponding minimum phase condition required by the KK algorithm. The results show

Optics EXPRESS

that without applying the KK detection, the EVM gradually improves with increasing the LO power. Such improvement is mainly attributed to the enhancement of the CSPR [44], which mitigates the effect of SSBI to some extent. In contrast, when applying the KK detection, the EVM always remains within the acceptable range, indicating that the KK processing is able to suppress SSBI and ensure the stability of the signal quality under different LO powers. It is noteworthy that excessive LO powers may introduce systematic nonlinear distortions that would degrade the overall performance of the system.

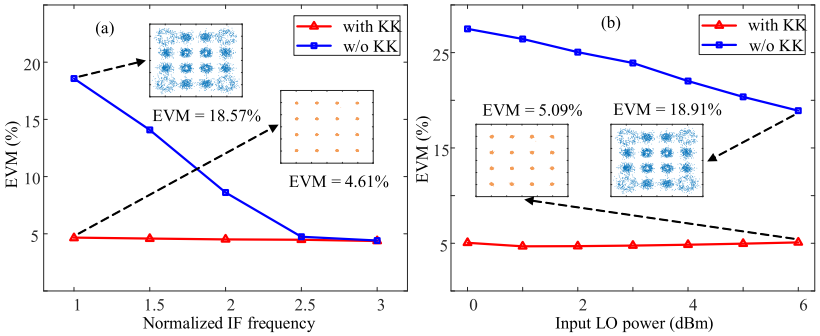

Fig. 5. (a) EVMs as a function of normalized IF frequency; (b) EVM versus input LO power. w/o: without.

Finally, since the AWG only allows us to configure the signal output in terms of peak-to-peak voltages, we test the proposed system by varying the input RF peak-to-peak voltage while keeping the LO frequency and power fixed at 14.75 GHz and 6 dBm, respectively. The results are presented in Fig. 6. As the RF power increases, the EVM without KK detection initially decreases and then increases. This behavior is attributed to the fact that SSBI power is proportional to the square of the input RF power and increases more rapidly than the power of the down-converted signal. For weaker RF signals, SSBI can be negligible, and increasing the input RF power improves the signal-to-noise ratio (SNR). However, once SSBI becomes dominant, further increases in RF power no longer improve EVM performance. With SSBI suppression provided by KK detection, the EVM performance, as shown in Fig. 6, is superior to that without KK detection. It should be highlighted that SSBI suppression can be further enhanced by increasing the CSPR. A higher CSPR strengthens the carrier component, benefiting the linearization of the detected signal and thus leading to the mitigation of SSBI in the direct detection systems. However, this improvement comes at the expense of receiver sensitivity, as allocating more power to the carrier reduces the power available for the modulated signal, leading to a lower SNR at the receiver.

The proposed photonic down-conversion approach employs a single DDMZM and eliminates the need for additional RF devices, thereby avoiding imbalance issues while still enabling the operations at higher frequencies and broader bandwidths. The conversion efficiency is measured to be approximately -17 dB as the RF and LO frequencies are varied from 3 GHz to 30 GHz, with the frequency difference between the LO and RF signals fixed at 500 MHz, when their respective power levels set at -5 dBm and 6 dBm. This method can also be extended to larger bandwidths as wideband DDMZMs become available. Due to the available signal generators, the spurious-free dynamic range is assessed by simulations using MATLAB 2020a and VPIphotonics 10.0, with parameters identical to those adopted in the experiments. The setup included a dual-frequency RF signal at 19.995 GHz and 20.005 GHz, and an LO signal at 18.5 GHz. The simulation results show that down-converted fundamental frequencies of 1.495 GHz and 1.505 GHz are generated, along with third-order intermodulation distortions (IMD3) at 1.49 GHz and 1.51 GHz. Figure 7 illustrates the power of these down-converted fundamental and IMD3 products as a function of input RF power, showing a spurious-free dynamic range (SFDR) of 113.36 dB·Hz2/3.

Optics EXPRESS

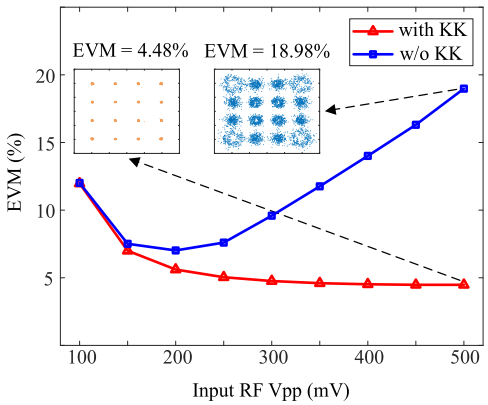

Fig. 6. EVM versus input RF peak-to-peak voltage (Vpp). w/o: without.

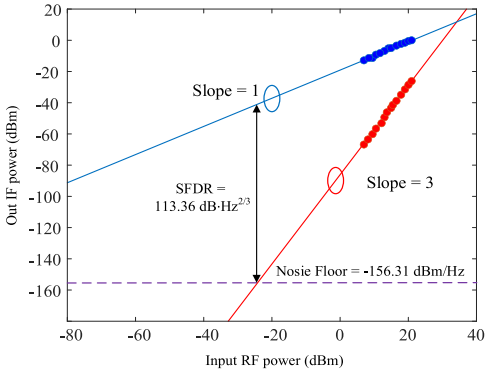

Fig. 7. Measured output IF power of fundamental term, IMD3, and versus input RF power.

In previous studies [39,40], the low IF reception of 16QAM broadband signals with their bandwidths of 2.3 GHz and 100 MHz was demonstrated, achieving EVM improvements of 9.5% and 8.79% respectively, through the KK processing. In comparison, our proposed scheme employs a simplified down-conversion structure that achieves a 13.96% EVM improvement for 16QAM signals with a 500 MHz bandwidth. Although the current experimental validation utilizes 500 MHz 16QAM signals for proof-of-concept demonstration, the proposed scheme is technically capable of supporting broadband reception, with potential applicability to signal bandwidths extending into the tens of GHz range, as supported by [36,37,45].

It is essential to highlight that the nonlinear operations involved in the KK algorithm including logarithmic and exponential functions effectively expand the signal bandwidth. Consequently, the KK algorithm necessitates a sampling rate that is several times higher than the Nyquist rate. This requirement can impose significant challenges on subsequent DSP operations, especially in terms of processing speeds and power consumption. Such challenges may limit the practical applicability of KK reception in broadband signal scenarios. To mitigate DSP complexity and enhance the feasibility of broadband signal reception, several techniques have been proposed in recent years. These include optimized KK algorithms [43, 46], iterative methods [47], and SSBI-free processing schemes [48].

Optics EXPRESS

4. Conclusion

A simplified low-IF RF receiver based on a PD is demonstrated, enabled by KK processing. A 16-QAM RF vector signal with a 500 MHz bandwidth is used to verify the low-IF reception performance of the system with and without KK processing, yielding EVMs of 4.61% and 18.57%, respectively, when there are no frequency gaps between the RF signal and the LO signal. This approach effectively reduces the bandwidth requirements for both the PD and DSP, offering significant potential for receiving high-frequency broadband RF signals in future communication and radar systems. Additionally, our microwave photonic down-conversion system, realized in a simplified and compact structure, provides a large instantaneous bandwidth, high conversion efficiency, and good linearity. By using a single-ended PD, the proposed receiver enables low-IF reception while reducing both cost and complexity.

Funding. National Natural Science Foundation of China (U22A2018, 62001072, 62222103); Project of Key Laboratory of Radar Imaging and Microwave Photonics (RIMP2019002).

Disclosures. The authors declare no conflicts of interest

Data availability. Data underlying the results presented in this paper are not publicly available at this time but may be obtained from the authors upon reasonable request

References

1. J. Yao, "Microwave photonic systems," J. Lightwave Technol. **40**(20), 6595–6607 (2022).
2. Z. Tang, Y. Li, J. Yao, *et al.*, "Photonics-based microwave frequency mixing: methodology and applications," Laser & Photonics Rev. **14**(1), 1800350 (2020).
3. R. Rady, C. Madsen, S. Palermo, *et al.*, "A 20–43.5-GHz wideband tunable silicon photonic receiver front-end for mm-wave channel selection/jammer rejection," J. Lightwave Technol. **41**(5), 1309–1324 (2023).
4. H. Chi, C. Wang, and J. Yao, "Photonic generation of wideband chirped microwave waveforms," IEEE J. Microw. **1**(3), 787–803 (2021).
5. W. F. Zhang, Y. Liu, and B. Wang, "Low-phase-noise ultra-wide arbitrary waveform generation using a wideband injection-locked optoelectronic oscillator," J. Lightwave Technol. **42**(21), 7693–7702 (2024).
6. P. Sen, J. V. Siles, N. Thawdar, *et al.*, "Multi-kilometre and multi-gigabit-per-second sub-terahertz communications for wireless backhaul applications," Nat. Electronics **6**(2), 164–175 (2023).
7. S. Pan and Y. Zhang, "Microwave photonic radars," J. Lightwave Technol. **38**(19), 5450–5484 (2020).
8. A. Batra, J. Barowski, D. Damyanov, *et al.*, "Short-range SAR imaging from GHz to THz waves," IEEE J. Microw. **1**(2), 574–585 (2021).
9. L. Yi, Y. Li, and T. Nagatsuma, "Photonic radar for 3D imaging: from millimeter to terahertz waves," IEEE J. Sel. Top. Quantum. Electron. **29**(5: Terahertz Photonics), 1–14 (2023).
10. G. Serafino, S. Maresca, C. Porzi, *et al.*, "Microwave photonics for remote sensing: from basic concepts to high-level functionalities," J. Lightwave Technol. **38**(19), 5339–5355 (2020).
11. H. C. Yu, M. H. Chen, H. B. Cao, *et al.*, "Simple photonic-assisted radio frequency down-converter based on optoelectronic oscillator," Photon. Res. **2**(4), B1–B4 (2014).
12. S. Zeng, J. Zhang, L. Li, *et al.*, "Broadband photonic-assisted microwave receiver with high cross-channel interference suppression and image rejection," Opt. Express **31**(10), 16833–16844 (2023).
13. V. R. Pagán and T. E. Murphy, "Electro-optic millimeter-wave harmonic downconversion and vector demodulation using cascaded phase modulation and optical filtering," Opt. Lett. **40**(11), 2481–2484 (2015).
14. L. Mackay, C. K. Lai, N. J. Athanasios, *et al.*, "Chip-based SBS for image rejection in a broadband microwave photonic mixer," Opt. Express **31**(3), 4268–4280 (2023).
15. Y. Zhou, J. Kong, F. Z. Zhang, *et al.*, "Microwave photonic I/Q mixer for wideband frequency downconversion with serial electro-optical modulations," Opt. Lett. **49**(1), 65–68 (2024).
16. Z. Tang, F. Zhang, D. Zhu, *et al.*, "A photonic frequency downconverter based on a single dual-drive Mach-Zehnder modulator," in *2013 IEEE International Topical Meeting on Microwave Photonics (MWP)*, 150–153 (2013).
17. Y. S. Gao, A. J. Wen, W. Chen, *et al.*, "All-optical, ultra-wideband microwave I/Q mixer and image-reject frequency down-converter," Opt. Lett. **42**(6), 1105–1108 (2017).
18. S. Zhu, X. J. Fan, M. Li, *et al.*, "Microwave photonic frequency down-conversion and channel switching for satellite communication," Opt. Lett. **45**(18), 5000–5003 (2020).
19. J. C. Li, S. G. Yang, H. W. Chen, *et al.*, "Fully integrated hybrid microwave photonic receiver," Photonics Res. **10**(6), 1472–1483 (2022).
20. W. L. Zhai, A. J. Wen, and D. J. Shan, "Linearized photonic microwave and mm-Wave mixer with dispersion-induced power fading compensation," IEEE Trans. Microwave Theory Tech. **68**(12), 5335–5346 (2020).
21. X. H. Gao, J. F. Du, G. J. Ji, *et al.*, "Filter-free photonic microwave I/Q modulator for reconfigurable frequency mixing," J. Lightwave Technol. **41**(9), 1–9 (2023).

Optics EXPRESS

22. S. T. Lipkowitz, T. U. Horton, and T. E. Murphy, "Wideband microwave electro-optic image rejection mixer," Opt. Lett. **44**(19), 4710–4713 (2019).
23. C. J. Huang, Z. L. Li, Y. F. Li, *et al.*, "Optoelectronic oscillator based microwave frequency downconverter with low phase noise and high conversion efficiency," J. Lightwave Technol. **43**(2), 530–538 (2022).
24. X. Li, A. Wen, X. Li, *et al.*, "Microwave photonic frequency down-conversion with self-interference cancellation and SSBI mitigation," Opt. Commun. **504**, 127391 (2022).
25. W. Wang, F. Li, Z. Li, *et al.*, "Dual-drive Mach-Zehnder modulator-based single side-band modulation direct detection system without signal-to-signal beating interference," J. Lightwave Technol. **38**(16), 4341–4351 (2020).
26. A. Mecozzi, C. Antonelli, and M. Shtaif, "Kramers–Kronig receivers," Adv. Opt. Photonics **11**(3), 480–517 (2019).
27. Z. Z. Tang and S. L. Pan, "A reconfigurable photonic microwave mixer using a 90° optical hybrid," IEEE Trans. Microwave Theory Tech. **64**(9), 3017–3025 (2016).
28. B. Lu, W. Pan, X. H. Zou, *et al.*, "Wideband microwave Doppler frequency shift measurement and direction discrimination using photonic I/Q detection," J. Lightwave Technol. **34**(20), 4639–4645 (2016).
29. D. Zhu, W. Chen, and S. L. Pan, "Photonics-enabled balanced Hartley architecture for broadband image-reject microwave mixing," Opt. Express **26**(21), 28022–28029 (2018).
30. J. W. Ding, Y. F. Wu, H. S. Yang, *et al.*, "Wideband image-reject RF channelization based on soliton microcombs," APL Photonics **8**(9), 090801 (2023).
31. W. Gou, J. Zhang, Z. Zhang, *et al.*, "Microwave photonics scanning channelizer with digital image-reject mixing and linearization," Opt. Commun. **528**, 129055 (2023).
32. Y. S. Gao, A. J. Wen, W. Zhang, *et al.*, "Ultra-wideband photonic microwave I/Q mixer for zero-IF receiver," IEEE Trans. Microwave Theory Tech. **65**(11), 4513–4525 (2017).
33. H. Zeng, R. Li, and W. Z. Li, "Simultaneous frequency up/down converting interface based on a single hardware incorporating two phase-correlated photonic mixers," Opt. Express **30**(6), 9643–9654 (2022).
34. T. Lin, Z. K. Zhang, J. G. Liu, *et al.*, "Reconfigurable photonic microwave mixer with mixing spurs suppressed and dispersion immune for radio-over-fiber system," IEEE Trans. Microwave Theory Tech. **68**(12), 5317–5327 (2020).
35. H. L. Li, J. C. Li, X. F. Li, *et al.*, "Complementary polarization-diversity coherent receiver for self-coherent homodyne detection with rapid polarization tracking,"," J. Lightwave Technol. **40**(9), 2773–2779 (2022).
36. A. Mecozzi, C. Antonelli, and M. Shtaif, "Kramers-Kronig coherent receiver," Optica **3**(11), 1220–1227 (2016).
37. T. Harter, C. Füllner, J. N. Kemal, *et al.*, "Generalized Kramers-Kronig receiver for coherent terahertz communications," Nat. Photonics **14**(10), 601–606 (2020).
38. C. Füllner, M. M. H. Adib, S. Wolf, *et al.*, "Complexity analysis of the Kramers–Kronig receiver," J. Lightwave Technol. **37**(17), 4295–4307 (2019).
39. C. Yin, J. Li, L. Shu, *et al.*, "Broadband lower-IF RF receiver based on microwave photonic mixer and Kramers-Kronig detection," Opt. Express **26**(20), 26400–26410 (2018).
40. Z. Tu, A. Wen, G. Yu, *et al.*, "A wideband photonic RF receiver with lower IF frequency enabled by Kramers–Kronig detection," J. Lightwave Technol. **37**(20), 5309–5316 (2019).
41. X. Gao, B. Xu, Y. Cai, *et al.*, "QAM modulation with single DDMZM based on direct-detection and Kramers-Kronig scheme in long reach PON," Opt. Fiber Technol. **48**, 289–296 (2019).
42. C. Yu, R. Gao, F. Wang, *et al.*, "Modified low CSPR Kramer-Kronig receivers based on a signal-signal beat interference estimation," Opt. Express **30**(16), 28251–28267 (2022).
43. S. Luo, J. Li, X. Yu, *et al.*, "An improved Kramers-Kronig receiver with upsampling-free and low carrier-to-signal power ratio," J. Lightwave Technol. **42**(19), 6731–6738 (2024).
44. C. Li, Y. Sun, M. Merklein, *et al.*, "Pilot-tone-assisted stimulated-Brillouin-scattering-based optical carrier recovery for Kramers-Kronig reception," J. Lightwave Technol. **40**(14), 4642–4648 (2022).
45. Z. Y. Wen, F. Yang, H. Jiang, *et al.*, "Modified Kramers-Kronig receiver based on memory polynomial compensation for photonics-assisted millimeter-wave communications," Opt. Express **31**(21), 34800–34816 (2023).
46. T. W. Bo and H. Kim, "Kramers-Kronig receiver operable without digital sampling," Opt. Express **26**(11), 13810–13818 (2018).
47. S. T. Le, V. Aref, K. Schuh, *et al.*, "Power-efficient single-sideband transmission with clipped iterative SSBI cancellation," J. Lightwave Technol. **38**(16), 4359–4367 (2020).
48. S. Ishimura, H. Y. Kao, K. Tanaka, *et al.*, "SSBI-free direct-detection system employing phase modulation for analog optical links," J. Lightwave Technol. **38**(9), 2719–2725 (2020).